

Mechanism of molecular interactions for tRNA^{Val} recognition by valyl-tRNA synthetase

SHUYA FUKAI,^{1,2,3} OSAMU NUREKI,^{1,2,3} SHUN-ICHI SEKINE,² ATSUSHI SHIMADA,^{1,3}
DMITRY G. VASSYLYEV,² and SHIGEYUKI YOKOYAMA^{1,2,3}

¹Department of Biophysics and Biochemistry, Graduate School of Science, The University of Tokyo, Bunkyo-ku, Tokyo 113-0033, Japan

²Cellular Signaling Laboratory and Structurome Group, RIKEN Harima Institute at SPpring8, Mikazuki-cho, Sayo, Hyogo 679-5148, Japan

³RIKEN Genomic Sciences Center, Tsurumi, Yokohama 230-0045, Japan

ABSTRACT

The molecular interactions between valyl-tRNA synthetase (ValRS) and tRNA^{Val}, with the C34-A35-C36 anticodon, from *Thermus thermophilus* were studied by crystallographic analysis and structure-based mutagenesis. In the ValRS-bound structure of tRNA^{Val}, the successive A35-C36 residues (the major identity elements) of tRNA^{Val} are base-stacked upon each other, and fit into a pocket on the α -helix bundle domain of ValRS. Hydrogen bonds are formed between ValRS and A35-C36 of tRNA^{Val} in a base-specific manner. The C-terminal coiled-coil domain of ValRS interacts electrostatically with A20 and hydrophobically with the G19-C56 tertiary base pair. The loss of these interactions by the deletion of the coiled-coil domain of ValRS increased the K_M value for tRNA^{Val} 28-fold and decreased the k_{cat} value 19-fold in the aminoacylation. The tRNA^{Val} K_M and k_{cat} values were increased 21-fold and decreased 32-fold, respectively, by the disruption of the G18-U55 and G19-C56 tertiary base pairs, which associate the D- and T-loops for the formation of the L-shaped tRNA structure. Therefore, the coiled-coil domain of ValRS is likely to stabilize the L-shaped tRNA structure during the aminoacylation reaction.

Keywords: RNA-protein interaction; aminoacyl-tRNA synthetase; tRNA; translation; X-ray crystallography

INTRODUCTION

The fidelity of protein synthesis is guaranteed by the specific recognition of amino acids and tRNAs by aminoacyl-tRNA synthetases (aaRSs). The aminoacylation of tRNA consists of two reaction steps: an active intermediate, aminoacyl-adenylate, is synthesized from the amino acid and adenosine triphosphate (ATP), and then, the aminoacyl moiety of the aminoacyl-adenylate is transferred to the 3'-terminal adenosine of the tRNA (Fersht and Kaethner 1976). The two-step aminoacylation reaction is catalyzed by the central catalytic domain of the aaRS. The 20 aaRSs are classified into two groups, classes I and II (10 members each), with completely distinct folds of the aminoacylation domains (Eriani et al. 1990). The class I aaRSs have an aminoacylation domain with the canonical Rossmann fold, where the cognate amino acid is distinguished from the noncognate

ones. Furthermore, the aminoacylation domains of the isoleucyl-, leucyl-, and valyl-tRNA synthetases (IleRS, LeuRS, and ValRS, respectively) have a large inserted domain, connective polypeptide 1 (CP1), involved in the proofreading/editing activity for additional fine discrimination of the amino acids (Lin et al. 1996; Nureki et al. 1998; Chen et al. 2000; Cusack et al. 2000; Fukai et al. 2000; Mursinna et al. 2001). We have determined the crystal structure of the ternary complex of a Val-AMP analog (*N*-[L-valyl]-*N'*-adenosyldiaminosulfone, designated as Val-AMS), ValRS, and tRNA^{Val}(CAC) from *Thermus thermophilus* (Fig. 1), and have elucidated the sophisticated mechanism for the discrimination of the cognate L-valine from the near-cognate L-isoleucine and L-threonine by the ValRS-tRNA^{Val} complex (Fukai et al. 2000).

The specific tRNA recognition occurs in the tRNA-binding domains, which have been appended to the Rossmann-fold domain in the evolutionary processes of class I aaRSs (Delarue and Moras 1993). The appended tRNA-binding domains recognize a small number of nucleotides that are conserved specifically in each cognate tRNA species for the discrimination between the cognate and noncognate tRNAs. These nucleotides are called identity elements, and constitute the identity set (Giegè et al. 1998). The major

Reprint requests to: Shigeyuki Yokoyama, Department of Biophysics and Biochemistry, Graduate School of Science, The University of Tokyo, 7-3-1 Hongo, Bunkyo-ku, Tokyo 113-0033, Japan; e-mail: yokoyama@biochem.s.u-tokyo.ac.jp.

Article and publication are at <http://www.rnajournal.org/cgi/doi/10.1261/rna.2760703>.

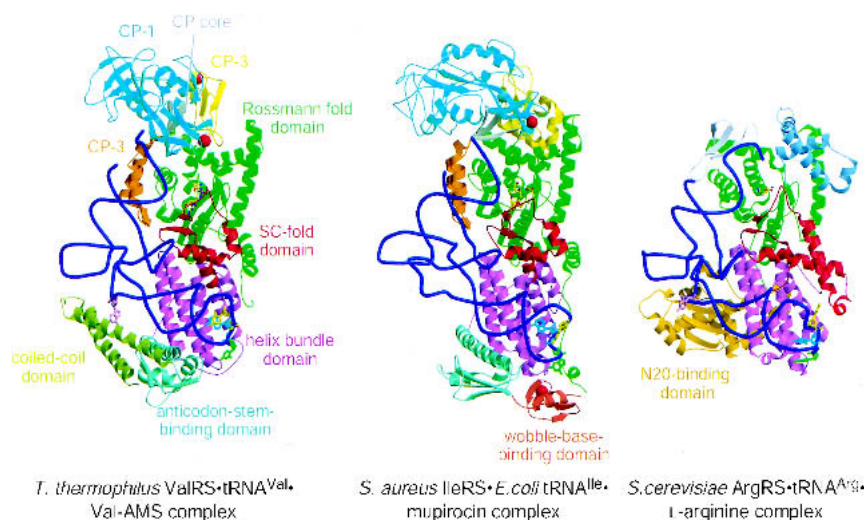


FIGURE 1. Crystal structures of the class Ia aaRS-tRNA complexes. The domains of the class Ia aaRS are colored as follows: Rossmann-fold (aminoacylation) domain, green; CP core, white; CP1 (editing) domain, cyan; CP2 domain, orange; CP3 domain, yellow; SC-fold domain, red; α -helix bundle domain, violet; anticodon-stem-binding domain, aquamarine; coiled-coil domain (ValRS), lime green; wobble-base-binding domain (IleRS), dark orange; N20-binding domain (ArgRS), dark orange; helical insertion (ArgRS), slate blue. Molecules bound to the Rossmann-fold domains are shown as ball-and-stick representations. Transfer RNAs are blue tubes. The first, second, and third anticodon nucleotides are shown as green, cyan, and yellow sticks, respectively. $\Psi 20$ of the tRNA^{Arg} is shown as pink sticks. Zinc ions are shown as red balls.

identity elements of tRNA^{Val} are A35 and C36 (the second and third nucleotides, respectively, of the anticodon) (Chu and Horowitz 1991; Pallanck and Schulman 1991; Tamura et al. 1991; Chu et al. 1992; Horowitz et al. 1999). ValRS has an α -helix bundle domain to recognize A35 and C36 on the anticodon loop of tRNA^{Val} (Fukai et al. 2000). The α -helix bundle domain is also found in IleRS (Nureki et al. 1998; Silvian et al. 1999), arginyl-tRNA synthetase (ArgRS; Cavarelli et al. 1998; Delagoutte et al. 2000; Shimada et al. 2001), methionyl-tRNA synthetase (MetRS; Mechulam et al. 1999; Sugiura et al. 2000), LeuRS (Cusack et al. 2000), and cysteinyl-tRNA synthetase (CysRS; T. Nakama, O. Nureki, and S. Yokoyama, in prep.; Newberry et al. 2002). These aaRSs constitute a subclass designated “class Ia” (Cusack 1995). In particular, ValRS (Fukai et al. 2000) and IleRS (Nureki et al. 1998; Silvian et al. 1999) are closely related to each other among the class Ia aaRS (Fig. 1). IleRS, LeuRS, MetRS, and ValRS recognize A35 of tRNA, whereas ArgRS and CysRS recognize C35.

In the present study, based on the improved structure of the *T. thermophilus* ValRS-tRNA^{Val}-Val-AMS ternary complex, the specific recognition mechanism of A35 and C36 of tRNA^{Val} by the α -helix bundle domain of ValRS was elucidated and compared with that of the specific recognition of A35 and U36 of *Escherichia coli* tRNA^{Ile} by the homologous domain of the *Staphylococcus aureus* IleRS in their ternary complex with mupirocin (Silvian et al. 1999). A further comparison with the ternary complex of yeast ArgRS, tRNA^{Arg}, and L-arginine (Fig. 1) sheds light on the

difference in the second anticodon letter recognition manner between the A35-recognizing and C35-recognizing aaRSs within class Ia. The *S. aureus* IleRS has a unique C-terminal zinc-binding domain, which is completely different from the C-terminal coiled-coil domain of the *T. thermophilus* ValRS (Fig. 1). Position 34, which is one of the identity elements of tRNA^{Ile} (Muramatsu et al. 1988; Pallanck and Schulman 1991; Nureki et al. 1994), is recognized by the IleRS C-terminal domain (Silvian et al. 1999), referred to hereafter as the “wobble-base-binding domain.” In contrast, the wobble base in position 34 is not an identity element of tRNA^{Val}, whereas the only major identity element other than A35-C36 is the discriminator, A73 (Pallanck and Schulman 1991; Horowitz et al. 1999). In the present study, we found that the C-terminal coiled-coil domain of ValRS is crucial for the aminoacylation, based on both the ValRS ternary complex structure and the structure-based mutagenesis of ValRS and tRNA^{Val}. The valylation activity depends on the tertiary interactions between the D- and T-loops, which are likely to be maintained by the coiled-coil domain in the ValRS-tRNA^{Val} complex. In addition, an X-ray crystallographic study of the ligand-free *T. thermophilus* ValRS reveals the dynamic change in the orientation of the coiled-coil domain relative to the α -helix bundle domain.

RESULTS AND DISCUSSION

Transfer RNA-binding architecture of ValRS

As shown in Figure 1, ValRS has the architecture conserved in the class Ia aaRSs for specific tRNA recognition (Fukai et al. 2000; Sugiura et al. 2000): the stem-contact fold (SC-fold) domain (colored red) and the following α -helix bundle domain (violet) are appended to the Rossmann-fold domain. In addition, the α -helix bundle domain connects with the following “anticodon-stem-binding” junction domain (colored aquamarine) and the C-terminal coiled-coil domain (lime green) in ValRS (Fig. 1). The anticodon-stem-binding domain (referred to hereafter as “AS-binding domain”) has also been found in the *S. aureus* IleRS structure (Fig. 1; Silvian et al. 1999). In the *T. thermophilus* ValRS-tRNA^{Val}-Val-AMS complex structure, the L-shaped tRNA^{Val} molecule is clamped between the SC-fold domain and the AS-binding and coiled-coil domains on the inner and outer sides, respectively.

Interaction of the tRNA D-stem with the SC-fold domain of ValRS

The SC-fold domain of ValRS forms a positively charged patch, which contacts the phosphate backbone of the D-stem of tRNA^{Val} (Fig. 2A). This contact between the ValRS SC-fold domain and the minor groove side of the tRNA^{Val} D-stem is consistent with the results of the footprinting analysis of *E. coli* tRNA^{Val} and ValRS (T. Niimi, O. Nureki, and S. Yokoyama, unpubl.). The two N_H groups of Arg570 hydrogen bond with the O2 atoms of C11 and C25, respectively (Fig. 2B). In most tRNA species, positions 11 and 25 are occupied by pyrimidine nucleotides, which have the O2 atom (Sprinzl et al. 1998). Whereas Arg570, forming the two hydrogen bonds, is not strictly conserved in most ValRSs, the electrostatic interaction between the SC-fold domain and the D-stem appears to be conserved and therefore related to the recognition of the common features of

the L-shaped tRNAs. A similar contact of the SC-fold domain with the tRNA D-stem has also been observed in the *S. aureus* IleRS·tRNA^{Ile}·mupirocin complex, in which the N_H groups of Gln640 and Gln706 of the *S. aureus* IleRS hydrogen bond with the O2 atoms of C11 and U12 of tRNA^{Ile}, respectively (Silvian et al. 1999). In IleRSs, these two positions corresponding to the Gln residues are normally occupied by hydrophilic residues, such as Glu and Arg. The mutation of the U12·A23 base pair on the D-loop of *E. coli* tRNA^{Ile} increases the *K_M* value for tRNA^{Ile} 24–29-fold (Nureki et al. 1994). However, the major groove side of A23 forms a tertiary interaction with A9, and therefore, the increase in the *K_M* value by the mutation of U12 is possibly due to the irregular conformation on the minor groove side of the U12·A23 base pair. Both ValRS and IleRS have polar interactions (electrostatic interaction and/or hydrogen bonding) of the SC-fold domain with the D-stem minor groove, which fit this domain on the inner side of the L-shaped tRNA structure.

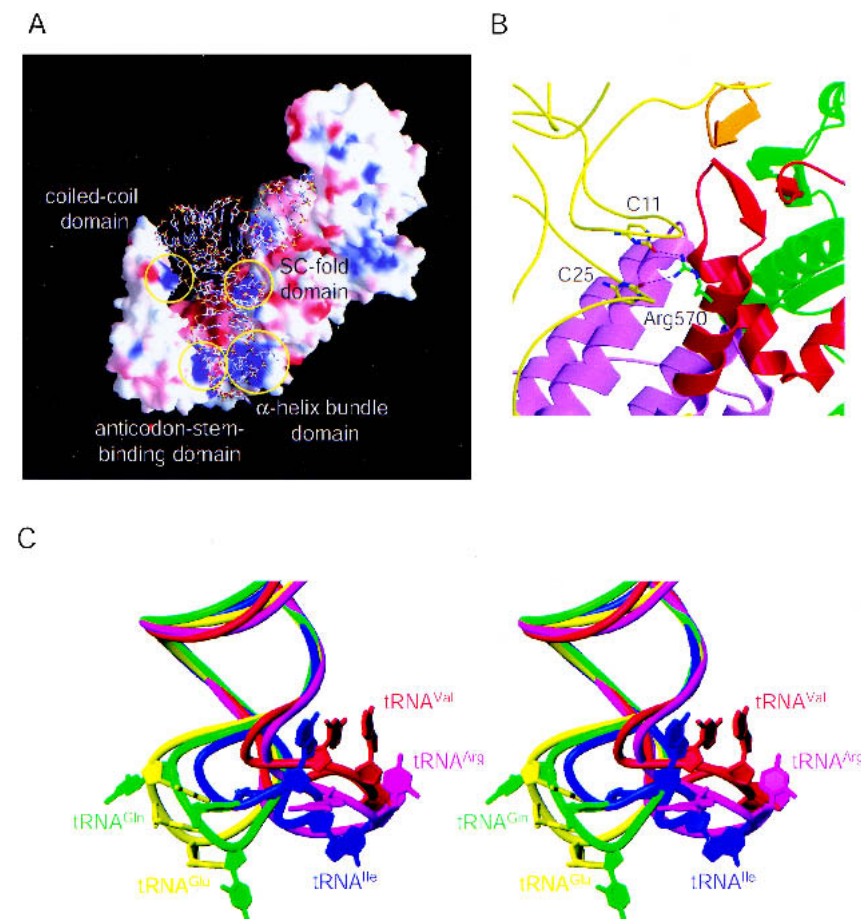


FIGURE 2. (A) Surface potential of the *T. thermophilus* ValRS. (B) Interactions of the ValRS SC-fold domain with the tRNA^{Val} D stem. Each domain of ValRS is colored as in Figure 1. The trace of the phosphorus atoms of tRNA^{Val} is shown as a yellow tube. C11 and C25 of tRNA^{Val} are shown as sticks, where the carbon atoms are yellow. Arg570 of ValRS is shown as sticks, where the carbon atoms are green. (C) The anticodon-loop structures of tRNAs bound to the class Ia and Ib aaRSs (stereoview). The phosphorous atoms of the anticodon stems are superposed. This figure shows the clear difference in the anticodon-loop structures between the tRNAs bound to the class Ia and Ib aaRSs.

Anticodon loop structure of tRNA^{Val}

The anticodon loop of tRNA^{Val} is extensively deformed, unwound, and bound to the bottom of the α-helix bundle domain on the minor groove side. The anticodon-loop conformation of the tRNA bound to the class Ia aaRS is quite different from that of the tRNA bound to the class Ib aaRS (Fig. 2C). In the *E. coli* GlnRS·tRNA^{Gln}·ATP complex structure, the tRNA^{Gln} anticodon loop is unwound toward the variable-loop side (Rould et al. 1991). The three anticodon bases of tRNA^{Gln} are splayed out, and fit into the separate pockets formed by the two β-barrel domains of GlnRS. In the *T. thermophilus* GluRS·tRNA^{Glu} complex structure (Sekine et al. 2001), the tRNA^{Glu} anticodon loop forms a U-turn, as observed in the crystal structure of *S. cerevisiae* tRNA^{Phe} (Sussman and Kim 1976). In the canonical U-turn structure, bases 32–33 as well as bases 34–38 are continuously stacked, and the loop is turned back between positions 33 and 34. In contrast, in the ValRS·tRNA^{Val}·Val-AMS complex structure, the intramolecular stacking interactions within the tRNA anticodon loop are disrupted, and the anticodon loop is unwound toward the D-loop side, as also shown in the *S. aureus* IleRS·tRNA^{Ile}·mupirocin complex (Silvian et al. 1999) and *S. cerevisiae* ArgRS·

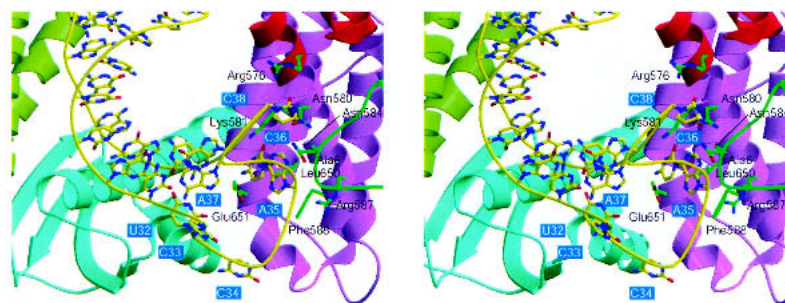
tRNA^{Arg}-L-arginine complex structures (Fig. 2C; Delagoutte et al. 2000).

Recognition of the tRNA^{Val} anticodon loop by the α -helix bundle domain of ValRS

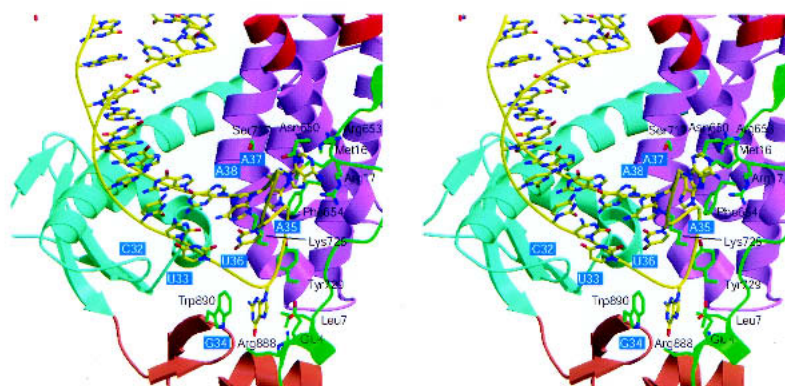
In the extensively deformed anticodon loop of tRNA^{Val}, C32, U33, and C34 are not well ordered, as shown by their high thermal factors ($>100 \text{ \AA}^2$), and their bases are splayed out along the sugar-phosphate backbone (Fig. 3A). These three nucleotides contact the corresponding nucleotides of the crystallographic symmetry-related tRNA^{Val} molecule in the crystal (data not shown). These crystal packing contacts are not likely to be related to the extensive deformation of the tRNA^{Val} anticodon loop, because a similar deformation of the anticodon loop has been observed in the complex structures of ArgRS•tRNA^{Arg}, arginine and IleRS•tRNA^{Ile}, mupirocin. Actually, this deformation of the anticodon loop is requisite for the base-specific recognition by ValRS, as described below. Position 34 of tRNA^{Val} is not the identity element of tRNA^{Val} (Pallanck and Schulman 1991; Horowitz et al. 1999). Correspondingly, C34 of tRNA^{Val} is exposed to the solvent, and is not recognized by ValRS (Fig. 3A), in the ValRS•tRNA^{Val}•Val-AMS complex structure.

In contrast, A35 and C36 are the major identity elements of tRNA^{Val} (Chu and Horowitz 1991; Pallanck and Schulman 1991; Tamura et al. 1991; Chu et al. 1992; Horowitz et al. 1999). In the ValRS•tRNA^{Val}•Val-AMS complex structure, A35 and C36 form a base-stacking interaction, and fit into a pocket formed by the first and third α -helices of the four-stranded α -helix bundle domain (Figs. 3A,C and 4A). This stacking interaction between A35 and C36 allows ValRS to recognize the successive AC sequence on the anticodon loop. Most natural tRNA species have neither A34-C35 nor A36-C37, because A34 is always modified to inosine, and position 37 is generally occupied by a purine nucleotide (Schulman and Pelka 1977; Sprinzl et al. 1998). Therefore, the recognition of the successive AC

A *T. thermophilus* ValRS•tRNA^{Val}(CAC)•Val-AMS complex



B *S. aureus* IleRS•*E. coli* tRNA^{Ile}(GAU)•mupirocin complex



C

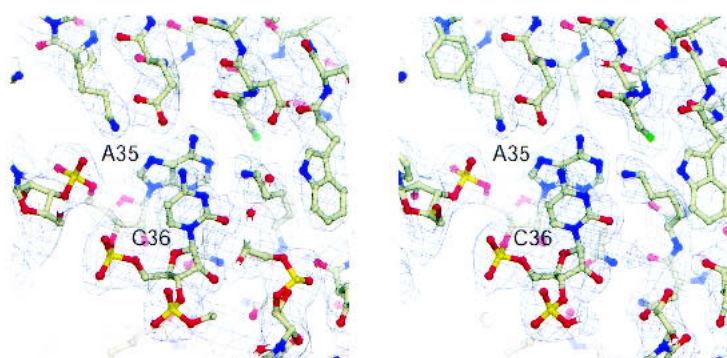


FIGURE 3. (A) Interactions between ValRS and the tRNA^{Val} anticodon arm (stereoview). Each domain of ValRS is colored as in Figure 1. The trace of the C1' atoms of tRNA^{Val} is shown as a yellow tube. The bases of tRNA^{Val} are shown as sticks, where the carbon atoms are yellow. The tRNA-interacting amino acid residues of ValRS are shown as sticks, where the carbon atoms are green. A35 and C36, which are the major identity elements of tRNA^{Val}, are recognized by the α -helix bundle domain. (B) Interactions between IleRS and the tRNA^{Ile} anticodon arm (stereoview). The representation is as in Figure 3A. G34 is recognized by the C-terminal wobble-base-binding domain. (C) σ_a -weighted $F_o - F_c$ omit map around A35 and C36 of tRNA^{Val}, contoured at the 5.0σ level (stereoview). A35, C36, and the surrounding amino acid residues were omitted. The atomic model of the ValRS•tRNA^{Val}•Val-AMS complex is shown as a ball-and-stick representation.

sequence around the tRNA anticodon may prevent the misrecognition of the noncognate tRNAs by ValRS. The A35 base forms van der Waals interactions with the Phe588 and

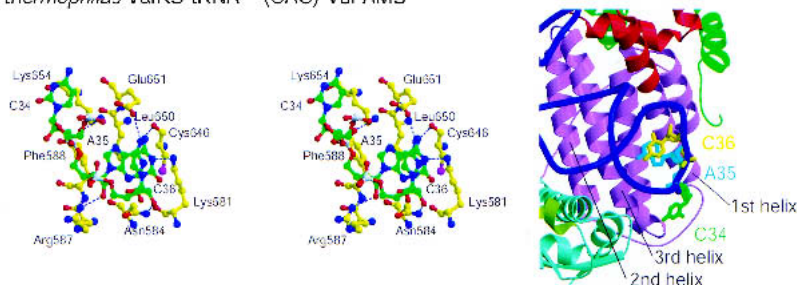
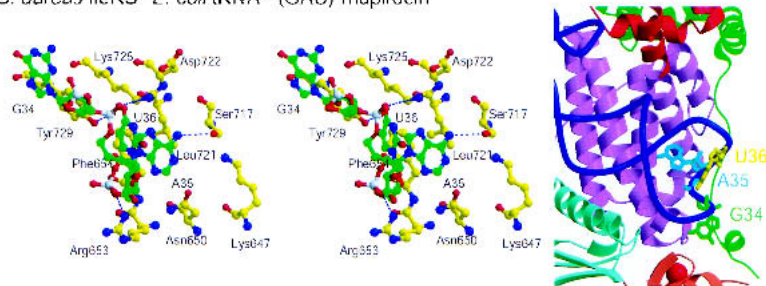
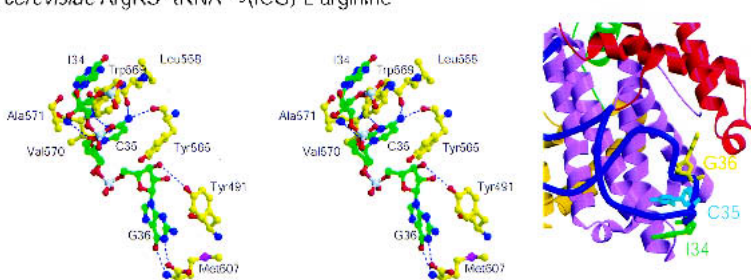
A *T. thermophilus* ValRS•tRNA^{Val}(CAC)•Val-AMSB *S. aureus* IleRS•*E. coli* tRNA^{Ile}(GAU)•mupirocinC *S. cerevisiae* ArgRS•tRNA^{Arg}(ICG)•L-arginine

FIGURE 4. Anticodon recognition by the class Ia aaRS. (A) *Left:* Ball-and-stick representation of the interactions between ValRS and the tRNA^{Val}(CAC) anticodon nucleotides (stereoview). The carbon atoms of the tRNA^{Val} anticodon nucleotides are green. The carbon atoms of the ValRS amino acid residues that interact with the anticodon nucleotides are yellow. *Right:* Overview of the position of the tRNA^{Val} anticodon nucleotides; representation as in Figure 1. (B) *Left:* Ball-and-stick representation of the interactions between IleRS and the tRNA^{Ile}(GAU) anticodon nucleotides (stereoview); representation same as in Figure 4A. *Right:* Overview of the position of the tRNA^{Ile} anticodon nucleotides; representation as in Figure 4A. (C) *Left:* Ball-and-stick representation of the interactions between ArgRS and the tRNA^{Arg}(ICG) anticodon nucleotides (stereoview); representation as in Figure 4A. *Right:* Overview of the position of the tRNA^{Arg} anticodon nucleotides; representation as in Figure 4A.

Leu650 side chains (Figs. 3A, 4A). The 6-NH₂ group of A35 hydrogen bonds with the α-CO group of Cys646 and the C₈OO⁻ group of Glu651. The N3 atom of C36 hydrogen bonds with the N_εH₂ group of Lys581. The N_ηH₂ group of Arg587 and the N_δH₂ group of Asn584 hydrogen bond with the 2'-OH groups of A35 and C36, respectively. Glu651 and Lys581 are completely conserved, and the other amino acid residues involved in the anticodon recognition are conserved or replaced by functionally equivalent amino acid residues (data not shown). The hydrogen bonds between ValRS and A35-C36 of tRNA^{Val} clearly demonstrate how ValRS recognizes the major identity elements of tRNA^{Val}.

The following A37 base is directed inward and stacks with

G39 (Fig. 3A). The orientation of A37 of tRNA^{Val} may disrupt the stacking interaction between U32 and C33 in the *T. thermophilus* ValRS•tRNA^{Val}•Val-AMS complex. Position 37 of tRNA^{Val} is usually occupied by N⁶-methyladenosine (m⁶A; Sprinzl et al. 1998). This small modification would not cause steric hindrance with any region of the tRNA^{Val} anticodon loop. C38 is flipped out, and is bound to a pocket formed by Arg576, Asn580, and Ala6. The base of C38 is intercalated between the side chains of Arg576 and Asn580. Arg576 is either conserved or replaced by Trp, and Asn580 is strictly conserved. Position 38 is occupied by adenosine in *E. coli* tRNA^{Val} (UAC). The substitution of G for A38 reduces the aminoacylation efficiency of the *E. coli* tRNA^{Val} by 12-fold, but that of C or U does not affect the aminoacylation efficiency (Horowitz et al. 1999). The 2-NH₂ group of G38 may cause steric hindrance with the pocket for position 38.

Comparison of the anticodon loop recognition by ValRS and IleRS

IleRS recognizes the first anticodon nucleotide in order to discriminate tRNA^{Ile} from tRNA^{Met} (Sprinzl et al. 1998). In the IleRS•tRNA^{Ile}•mupirocin complex, G34 is flipped out, and interacts with the C-terminal, wobble-base-binding domain (Fig. 3B). Intriguingly, the wobble-base-binding domain of IleRS is replaced by the coiled-coil domain of ValRS, which interacts electrostatically with A20 and hydrophobically with the G19•C56 tertiary base pair in the ValRS•tRNA^{Val}•Val-AMS complex structure, as described below.

Both IleRS and ValRS recognize the second and third anticodon nucleotides. Particularly, the second anticodon nucleotides of tRNA^{Ile} and tRNA^{Val} are adenosine. Superposition of the α-helix bundle domains (r.m.s.d. 1.7 Å over 114 C_α atoms) of the *S. aureus* IleRS and the *T. thermophilus* ValRS shows that the spatial arrangements of the anticodon-interacting amino acid residues are well conserved (Fig. 4A,B). However, the manner of the anticodon recognition by ValRS is unexpectedly different from that by IleRS. The position of A35 of tRNA^{Ile} in the binding pocket is shallower than that of tRNA^{Val}. This difference may be ascribed to the different recognition manners of the 6-NH₂

group of A35 between tRNA^{Ile} and tRNA^{Val}. The A35 6-NH₂ group of tRNA^{Ile} forms only one hydrogen bond with IleRS, whereas that of tRNA^{Val} forms two hydrogen bonds with ValRS (Fig. 4A,B). Asp722 of the *S. aureus* IleRS, which corresponds to Glu651 of the *T. thermophilus* ValRS, does not hydrogen bond with any nucleotides. The Glu residue is conserved among the ValRSs from all organisms. In contrast, Asp722 of the *S. aureus* IleRS is conserved among only the prokaryotic-type IleRSs, and is replaced by Arg among the eukaryotic-type IleRSs. The Asp and Arg residues of IleRS may be unable to interact with A35 of tRNA^{Ile}, because their side chains are too short and too long, respectively, compared with the length of the corresponding Glu residue of ValRS.

In the *S. aureus* IleRS·tRNA^{Ile}·mupirocin complex, U36 is not base-stacked with A35, and is not recognized by IleRS (Figs. 3B, 4B). The 3-NH group of U36 forms a hydrogen bond with the 2-CO group of U33. All tRNA^{Ile} species have uridine at position 33 (Sprinzl et al. 1998). The base of U33 is stacked with that of A38, which projects towards the inside of the anticodon loop without disrupting the stacking interaction between C32 and U33, in the *S. aureus* IleRS·*E. coli* tRNA^{Ile}·mupirocin complex. Concomitantly, A37 is bulged out in the *S. aureus* IleRS·*E. coli* tRNA^{Ile}·mupirocin complex (Fig. 3B), probably because position 37 of *E. coli* tRNA^{Ile} is occupied by a hypermodified nucleotide, t⁶A (N⁶-threonylcarbamoyladenosine; Parthasarathy et al. 1977; Sprinzl et al. 1998). If t⁶A at position 37 were directed inward and stacked with the base at position 39, as in the case of the ValRS·tRNA^{Val}·Val-AMS complex, then the bulky threonylcarbamoyl group might cause steric hindrance with the phosphate backbone. Therefore, the degree of modification at position 37 appears to be responsible for whether the orientation of the modified base is either inward or outward.

A35-recognizing class Ia aaRSs and C35-recognizing class Ia aaRSs

IleRS, ValRS, LeuRS, and MetRS recognize A35, whereas the other class Ia aaRSs, ArgRS and CysRS, recognize C35. Correspondingly, the position of the C35 recognition pocket of ArgRS (Delagoutte et al. 2000) is different from that of the A35 recognition pockets of ValRS and IleRS (Fig. 3A,B). The α -helix formed by residues 547 to 567 in *S. cerevisiae* ArgRS is shorter than the corresponding α -helices of IleRS and ValRS (residues 701 to 730 in the *S. aureus* IleRS, and residues 630 to 658 in the *T. thermophilus* ValRS) by two turns (Fig. 4). The last two turns of IleRS and ValRS are replaced by a loop structure (residues 560 to 573 in the *S. cerevisiae* ArgRS), which forms the C35-recognition pocket of ArgRS (Fig. 4C). In contrast, the A35-recognition pockets of IleRS and ValRS are formed on the first and third α -helices of the α -helix bundle domain. In addition, Leu650 of

the *T. thermophilus* ValRS and Leu721 of the *S. aureus* IleRS are replaced by Tyr565 of the *S. cerevisiae* ArgRS, which occupies the position corresponding to that of the A35 recognition pockets of IleRS and ValRS (Fig. 4). Tyr565 of the *S. cerevisiae* ArgRS seems to shift C35 of tRNA^{Arg}, compared with A35 of tRNA^{Ile} and tRNA^{Val}. C35 of tRNA^{Arg} is stacked with the Trp569 side chain of the *S. cerevisiae* ArgRS. The remarkable difference in the pocket for the second anticodon nucleotide suggests that the A35-recognizing class Ia aaRS could not be converted to the C35-recognizing class Ia aaRS by simple replacements of amino acid residues, and vice versa.

Interactions between the AS-binding domain of ValRS and the tRNA^{Val} anticodon stem

The many interactions between ValRS and the tRNA^{Val} anticodon loop may indirectly distort the structure of the tRNA^{Val} anticodon stem, where the planarities of the C27·G43 and U28·A42 base pairs are impaired (Fig. 3A). A previous biochemical study showed that the stiffening of the anticodon stem by the introduction of five consecutive C·G base pairs caused a 50-fold decrease in the aminoacylation efficiency of *E. coli* tRNA^{Val} (Horowitz et al. 1999). The distortion of the C27·G43 and U28·A42 base pairs in the *T. thermophilus* tRNA^{Val} explains the importance of the anticodon stem flexibility. The anticodon stem of tRNA^{Val} interacts with the AS-binding domain of ValRS. The first α -helix and the following loop of the AS-binding domain of ValRS form van der Waals interactions with the tRNA^{Val} anticodon stem on the minor groove side (Figs. 3A, 5A). There is no hydrogen bond between the AS-binding domain and the tRNA^{Val} anticodon stem. Nevertheless, a positively charged patch on the surface of the AS-binding domain forms electrostatic interactions with the negatively charged phosphate groups of the tRNA^{Val} anticodon stem (Fig. 2A). The orientation of the AS-binding domain is fixed by the van der Waals interactions between the first helix of the AS-binding domain and the second helix of the α -helix bundle domain (Fig. 3A). The AS-binding domain of ValRS may function as a “splint” for the distorted anticodon stem (Fig. 5). The deletion mutant of both the AS-binding and coiled-coil domains [Δ (712–862)] completely abolished the aminoacylation activity of the *T. thermophilus* ValRS without loss of the thermal stability (data not shown), probably due to the lack of the interaction with the anticodon stem of tRNA. Actually, ArgRS, which intrinsically lacks the AS-binding domain, can shift the positioning of the essential tRNA^{Arg} anticodon nucleotides for the arginylation toward the 5' side by one nucleotide (Kiga et al. 2001). Not only the α -helix bundle domain but also the following AS-binding domain is conserved between ValRS and IleRS, despite the low similarity in the primary structures of their AS-binding domains (Fig. 5B). Although the orientation of the IleRS AS-binding domain relative to the α -helix bundle domain is

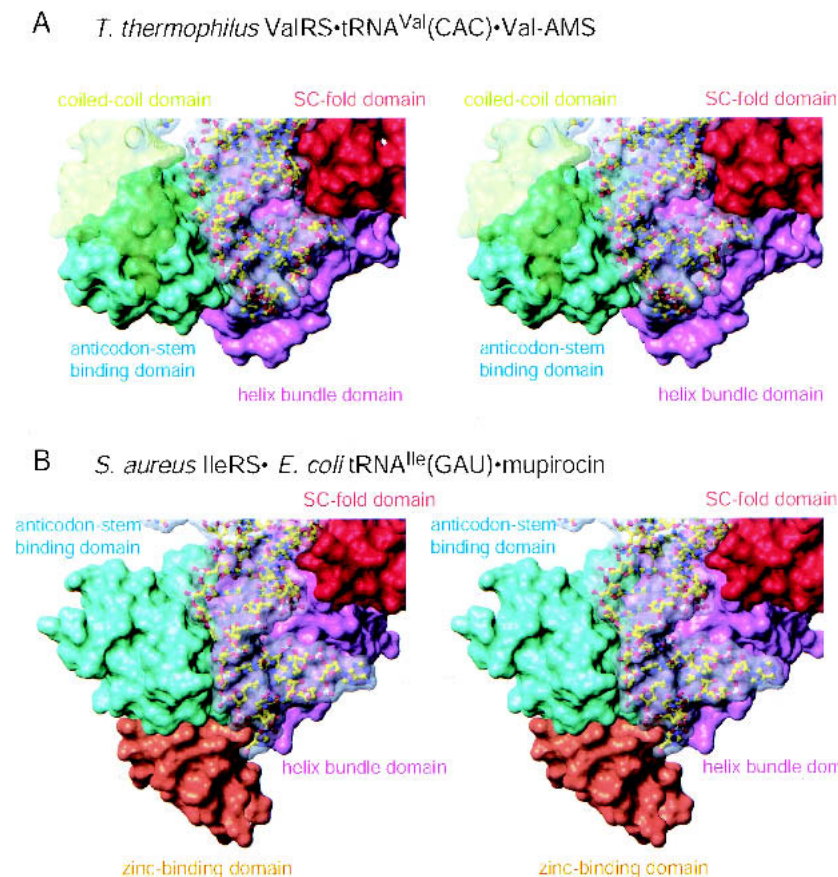


FIGURE 5. (A) Interactions between ValRS and the tRNA^{Val} anticodon stem (stereoview). Each domain of ValRS is shown as a contact surface colored as in Figure 1. The tRNA^{Val} is shown as a ball-and-stick representation with the contact surface colored translucent white. (B) Interactions between IleRS and the tRNA^{Ile} anticodon stem (stereoview); representation as in Figure 5A.

slightly different from that of the ValRS AS-binding domain, both AS-binding domains interact with the tRNA anticodon stem in a similar manner (Fig. 5).

Interactions of the C-terminal coiled-coil domain with the D- and T-loops of tRNA^{Val}

The C-terminal coiled-coil domain also has a positively charged region (Fig. 2A), which interacts with a single-stranded RNA region, or the “variable pocket” (McClain and Foss 1988), formed by the D- and T-loops (Fig. 6A). This interaction has been implied by biochemical studies of yeast and *E. coli* tRNA^{Val} species (Vlassov et al. 1983; Horowitz et al. 1999). The “variable pocket”, which comprises nucleotides 16, 17, 20, 59, and 60, forms an arch protruding from the tRNA surface (McClain and Foss 1988). A20 of tRNA^{Val} interacts with the coiled-coil domain of ValRS (Fig. 6A), which is missing in the other class Ia aaRSs. The A20 base is intercalated between the side chains of Arg843 and Leu815. The N1 atom of A20 hydrogen bonds with the side-chain N_δH₂ group of Asn847. The 2'-

OH group of A20 hydrogen bonds with the N_ηH₂ group of Arg818. The backbone phosphates of A20 and A21 form salt bridges with the N_ηH₂ groups of Arg843 and Arg818, respectively. These two Arg residues are either conserved or replaced by Lys; the Asn residue is not conserved. Two other *T. thermophilus* tRNA^{Val} isoacceptors, which were not used in this study, have cytidine and uridine, respectively, at position 20 (data not shown). Therefore, the hydrophilic interactions with position 20 (rather than the specific recognition of position 20) are likely to play an important role. Furthermore, the G19•C56 tertiary base pair of tRNA^{Val} interacts with the hydrophobic face formed by Pro833 and Val836, which are highly conserved in the ValRSs (Fig. 6A). This hydrophobic interaction seems to stabilize the G19•C56 tertiary base pair, which associates the D- and T-loops of the tRNA, together with the G18•Ψ55 tertiary base pair.

Mutational analyses of ValRS and tRNA^{Val}(CAC)

To investigate the function of the C-terminal coiled-coil domain, we carried out mutational analyses of ValRS, using the tRNA^{Val}(CAC) transcript and mature tRNA^{Val} purified from *T. thermophilus*. We first analyzed a deletion mutant, Δ(795–862), which lacks the coiled-coil domain (Table 1). The aminoacylation activity of the Δ(795–862) mutant was drastically reduced compared with that of the wild type. The deletion of residues 795–862 not only increased the *K_M* values 28-fold and 51-fold, but also decreased the *k_{cat}* values 19-fold and 72-fold, for the in vitro transcribed and mature tRNA^{Val}s, respectively. Subsequently, we analyzed an R818A/R843A double mutant, where Arg818 and Arg843 are replaced by Ala, to confirm the importance of the two salt bridges between the two Arg residues and the tRNA^{Val} phosphate backbone. The R818A/R843A mutation increased the *K_M* values 21-fold and 26-fold for the in vitro transcribed and mature tRNA^{Val}s, respectively, but not their *k_{cat}* values. The increase in the *K_M* value by the R818A/R843A mutation was almost comparable to that caused by the deletion of the coiled-coil domain (Table 1). These results clearly show that the two Arg residues, Arg818 and Arg843, play a primary role in forming the stable ValRS•tRNA^{Val} complex, and suggest that the other part of the coiled-coil domain, possibly the aforementioned

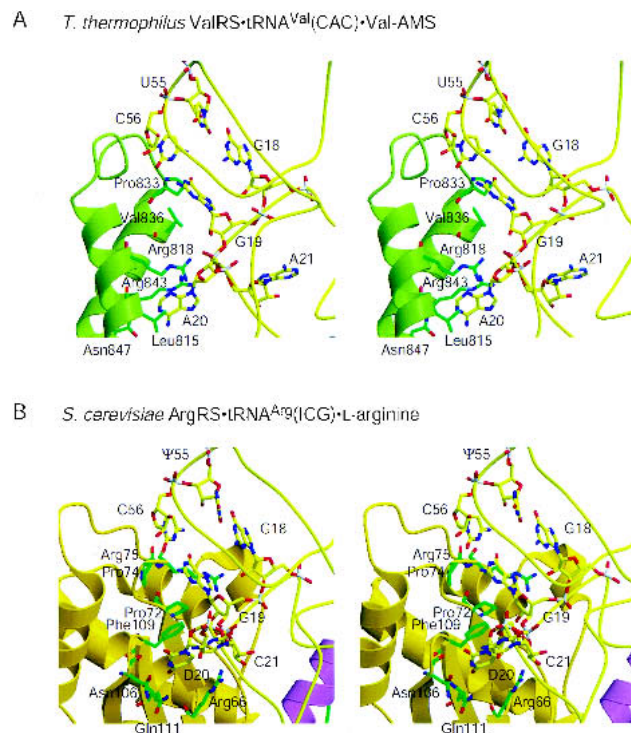


FIGURE 6. Interactions with the D- and T-loops of tRNA. (A) Interactions between the ValRS coiled-coil domain and tRNA^{Val} (stereoview). The trace of the phosphorus atoms of tRNA^{Val} is shown as a yellow tube. A20, U18•G55, and C19•G56 of tRNA^{Val} are shown as a ball-and-stick representation, where the carbon atoms are yellow. The ValRS coiled-coil domain is lime green. The ValRS amino acid residues that interact with the D- and T-loops of tRNA^{Val} are shown as a ball-and-stick representation, where the carbon atoms are green. (B) Interactions between the ArgRS N20-binding domain and tRNA^{Arg} (stereoview). The representation is the same as in Figure 6A, except that the ArgRS N20-binding domain is dark yellow.

G19•C56 binding pocket, is crucial for the catalytic processes, such as the correct positioning of the CCA end in the aminoacylation catalytic site.

We also analyzed tRNA^{Val} mutants that either partially or completely lack tertiary interactions between the D- and T-loops (Table 1). If the D-loop-T-loop interaction is crucial and stabilized by the coiled-coil domain, then the lack of the interaction should reduce the aminoacylation efficiency as well as the aforementioned ValRS mutations, $\Delta(795-862)$ and R818A/R843A. Actually, a point mutation at position 18 (G18U) and that at position 19 (G19C) increased the K_M values for tRNA by about 10- and 20-fold, respectively. The G19C mutant had a slightly smaller k_{cat} value than the wild type. The aminoacylation activity of the G19C mutant could be recovered by the introduction of the C56G mutation (G19C/C56G), with a slight increase in the K_M value. The G19C/C56G variant retains the tertiary loop-loop interactions, because the nucleotides at positions 19 and 56 form a Watson-Crick tertiary base pair. The recovery of the aminoacylation efficiency by the G19C/C56G mutation is ascribed to the acquisition of the C19•G56 tertiary

base pair, in place of the normal G19•C56 tertiary base pair. Therefore, we conclude that the tertiary loop-loop interactions are crucial for the efficient aminoacylation by ValRS. However, the partial disruption of the loop-loop interactions reduced the aminoacylation efficiency less than did $\Delta(795-862)$. A very marked reduction in the aminoacylation efficiency was caused by the double mutation at positions 18 and 19 (G18U/G19C). The G18U/G19C mutation increased the K_M value 21-fold, and decreased the k_{cat} value by 30-fold. This reduction in the aminoacylation efficiency is comparable to that caused by $\Delta(795-862)$.

The ValRS-tRNA^{Val}•Val-AMS complex structure and the mutational analyses suggest that the reduction in the aminoacylation efficiency caused by $\Delta(795-862)$ is due to the absence of the tertiary loop-loop interaction of tRNA^{Val}. The posttranscriptional modification of tRNA^{Val} seems unable to suppress this absence of the interaction caused by the deletion of the ValRS coiled-coil domain, although the modification is likely to stabilize the D-loop-T-loop interaction (Derrick and Horowitz 1993). The partial disruption of the tertiary interactions was suggested by an NMR spectroscopic analysis of ¹⁹F-labeled tRNA^{Val} and its complex with ValRS (Chu and Horowitz 1991). This partial disruption is probably prevented from extending to complete disruption by the interactions between the ValRS coiled-coil domain and the G19•C56 tertiary base pair of tRNA^{Val}. These results imply that the coiled-coil domain of ValRS holds the partially disrupted tertiary base pairs, but not the completely disrupted base pairs, and subsequently maintains the canonical L-shaped structure of tRNA^{Val}.

Interactions with the nucleotide at position 20 of tRNA^{Val} and tRNA^{Arg}

Adenosine at position 20 is the major identity element of most tRNA^{Arg} species (McClain and Foss 1988; Shimada et al. 2001), and is recognized by the N-terminal domain of ArgRS (Delagoutte et al. 2000; Shimada et al. 2001), which has a completely different structure from that of the position 20-interacting ValRS coiled-coil domain. Actually, the specific A20 recognition by the N-terminal domain of ArgRS differs from the electrostatic interactions between the ValRS coiled-coil domain and position 20 of tRNA^{Val}. Moreover, the orientation of the ArgRS N-terminal domain is fixed by the hydrophobic interactions with the α -helix bundle domain (Shimada et al. 2001), whereas there is no interdomain interaction that stabilizes the orientation of the ValRS coiled-coil domain (Fukai et al. 2000). These structural and functional differences in the A20-binding domain between ArgRS and ValRS can be ascribed to their distinct evolutionary origins. Our crystallographic analysis of the ligand-free ValRS yielded clear electron densities for the AS-binding domain and the coiled-coil domain (Fig. 7), although we could not complete the structure refinement ($R_{work}=0.316/R_{free}=0.383$, 10–4.0 Å resolution) because of

TABLE 1. The kinetic analyses of the *T. thermophilus* ValRS and tRNA^{Val} (CAC) mutants

ValRS Transcript	$K_M(\text{tRNA})$ (μM)	k_{cat} (sec^{-1})	k_{cat}/K_M ($\text{sec}^{-1} \cdot \mu\text{M}^{-1}$) (relative)
Wild-type	1.5 ± 0.44	6.7 ± 2.0	4.4 (1)
$\Delta(795-862)$	42 ± 8.2	0.36 ± 0.16	8.5×10^{-3} (1.9×10^{-3})
R818A/R843A	31 ± 14	4.3 ± 1.3	1.4×10^{-1} (3.2×10^{-2})
Native	$K_M(\text{tRNA})$ (μM)	k_{cat} (sec^{-1})	k_{cat}/K_M ($\text{sec}^{-1} \cdot \mu\text{M}^{-1}$) (relative)
Wild-type	0.70 ± 0.21	1.3 ± 0.40	1.9 (1)
$\Delta(795-862)$	36 ± 1.6	$1.8 \times 10^{-2} \pm 9.4 \times 10^{-3}$	5.0×10^{-4} (2.6×10^{-4})
R818A/R843A	18 ± 7.3	1.1 ± 0.12	6.1×10^{-2} (3.2×10^{-2})
tRNA ^{Val} (CAC) transcript	$K_M(\text{tRNA})$ (μM)	k_{cat} (sec^{-1})	k_{cat}/K_M ($\text{sec}^{-1} \cdot \mu\text{M}^{-1}$) (relative)
Wild-type	1.5 ± 0.44	6.7 ± 2.0	4.4 (1)
G18U	13 ± 5.6	4.2 ± 1.1	3.2×10^{-1} (7.2×10^{-2})
G19C	27 ± 1.5	1.2 ± 0.3	4.4×10^{-2} (1.0×10^{-2})
G18U/G19C	31	0.21	6.8×10^{-3} (1.5×10^{-3})
G19C/C56G	5.5 ± 0.4	5.3 ± 0.1	9.6×10^{-1} (2.2×10^{-1})

the insufficient quality of the diffraction data and the partial disorder of the CP1 domain. The electron density (Fig. 7B) shows that the AS-binding domain and the coiled-coil domain of the ligand-free ValRS are opened outward, compared with the ValRS-tRNA^{Val}-Val-AMS complex (Fig. 7A). In the complex, the two C-terminal domains are anchored mostly through interactions with the tRNA (Figs. 1, 5A). In the present open form of the ligand-free ValRS, the tip of the coiled-coil domain is fixed by the crystal packing (Fig. 7B). Therefore, it may be possible that the coiled-coil domain of the tRNA-free ValRS in solution is more flexible and moves upon tRNA^{Val} binding so as to hold the D- and T-loops. In contrast, the C-terminal domains of the tRNA-free IleRS (Nureki et al. 1998) and LeuRS (Cusack et al. 2000) are disordered in their crystal structures. The flexible coiled-coil domain of ValRS sharply contrasts with the firmly fixed N-terminal domain of ArgRS (Shimada et al. 2001), although these domains recognize similar parts of the tRNA (Fig. 6).

However, there are some similarities between the ArgRS N-terminal domain and the ValRS coiled-coil domain (Fig. 6A,B). As described above, the ValRS coiled-coil domain interacts electrostatically with position 20 and hydrophobically with the G19-C56 tertiary base pair in the ValRS-tRNA^{Val}-Val-AMS complex structure. We also found similar contacts in the *S. cerevisiae* ArgRS-tRNA^{Arg}-L-arginine complex structure (Delagoutte et al. 2000). The N-terminal domain forms hydrogen bonds with posi-

tion 20, and interacts hydrophobically with the G19-C56 tertiary base pair (Fig. 6B). By analogy with the present kinetic and crystallographic studies of the *T. thermophilus* ValRS and tRNA^{Val}, one could imagine that the ArgRS N-terminal domain maintains the L-shape of tRNA^{Arg}.

MATERIALS AND METHODS

Structural refinement of the *T. thermophilus* ValRS-tRNA^{Val}-Val-AMS complex

To improve the main-chain geometry of the *T. thermophilus* ValRS-tRNA^{Val}-Val-AMS complex structure (PDB code 1GAX),

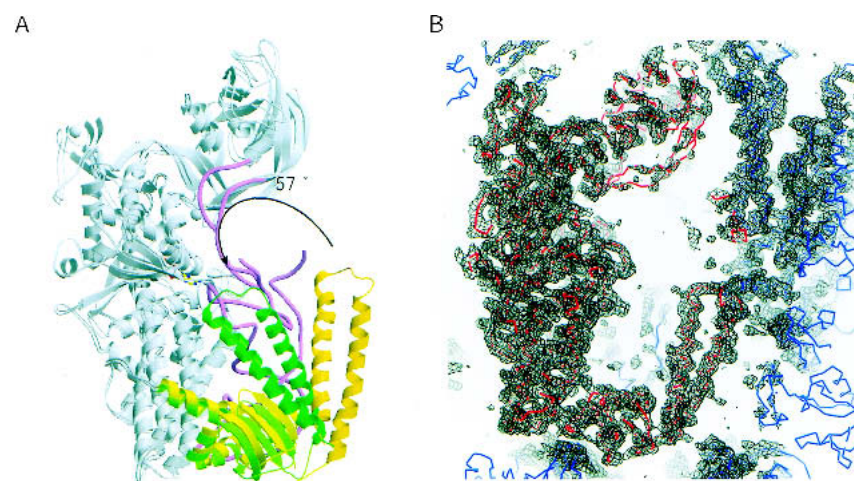


FIGURE 7. Change in the orientation of the ValRS coiled-coil domain. (A) Structural comparison between the tRNA^{Val}-bound ValRS and the ligand-free ValRS. The Rossmann-fold domains are superposed. The coiled-coil domains of the tRNA^{Val}-bound ValRS and the ligand-free ValRS are yellow and green, respectively. The AS-binding domains of the tRNA^{Val}-bound ValRS and the ligand-free ValRS are light yellow and light green, respectively. This figure suggests the dynamic movement of the coiled-coil domain. (B) A solvent-flattened and NCS-averaged F_o electron density map of ValRS, contoured at the 1.0σ level.

we reexamined the ambiguous regions, including residues 94 to 104 and 235 to 237, and manually modified them. Further structural refinement after this modification improved the main-chain geometry of the ValRS structure, although it had slightly higher R_{work} and R_{free} factors (24.7% and 28.1%, respectively) than those of the previous ValRS complex structure (Fukai et al. 2000). C32-U33-C34 and C74-C75 of tRNA^{Val} and the currently improved regions of ValRS are not well ordered, which may have resulted in the relatively high R_{work} and R_{free} values. The core, the allowed, the generously allowed, and the disallowed regions in the further-refined ValRS-tRNA^{Val}-Val-AMS complex structure comprise 80.0%, 18.1%, 1.7%, and 0.2%, respectively, of the ValRS amino acid residues, whereas those in the previous structure comprised 78.6%, 19.4%, 1.7%, and 0.3%, respectively. At 2.9 Å resolution, we consider a structure with better main-chain geometry and a slightly higher R factor to be more accurate than that with worse main-chain geometry and a slightly lower R factor. The refinement procedure was described by Fukai et al. (2000). The coordinates of this further-refined ValRS-tRNA^{Val}-Val-AMS complex structure with better main-chain geometry have been deposited in the Protein Data Bank, with the PDB code 1IVS.

Crystallographic and structural analyses of the *T. thermophilus* ligand-free ValRS

Small, very thin crystals ($100 \times 20 \times \sim 5 \mu\text{m}^3$) of the ligand-free ValRS were grown at 20°C by the hanging-drop vapor diffusion method over a period of 1 mo. Ligand-free ValRS crystals suitable for data collection ($200 \times 50 \times \sim 10 \mu\text{m}^3$) were obtained by using a macro-seeding method. The ValRS solution for crystallization was prepared at a final protein concentration of 10–20 mg/mL. The ValRS solution (1 μL) was mixed with 1 μL of the crystallization solution, containing 50 mM ADA·Na (*N*-[2-acetoamide]iminodiacetic acid sodium salt) buffer (pH 6.5) containing 2% 2-propanol, 100 mM lithium sulfate, and 12% polyethylene glycol (PEG) 4000. The drop solution was slowly equilibrated against the reservoir solution, 50 mM ADA·Na buffer (pH 6.5) containing 2% 2-propanol, 100 mM lithium sulfate, and 14% PEG4000. For data collection under cryo-conditions, the ValRS crystal was transferred to a mother liquor containing 20% ethylene glycol before flash cooling. The data collection was carried out at 90 K at station BL44XU, SPring8, Harima, Japan ($\lambda=0.900$ Å). The data set was processed with the programs DENZO and SCALEPACK (Otwinowski and Minor 1997). The ValRS crystal belongs to the space group $P2_12_12_1$, with unit cell parameters of $a=186.6$ Å, $b=207.3$ Å, $c=59.23$ Å. We observed 62,536 total reflections and 19,052 unique reflections up to 4.0 Å resolution. The values of R_{sym} , completeness, and $\langle I \rangle / \langle \sigma \rangle$ were 0.144 (0.396), 0.938 (0.894), and 4.6 (2.4), respectively, where the values in parentheses correspond to the highest resolution shell (4.07–4.0 Å). Subsequent processes were carried out with the CCP4 program suite (CCP4 1994). The initial phase was determined by the molecular replacement method, using the *T. thermophilus* ValRS structure (PDB code 1GAX) as a search model. Solutions of the rotation and translation functions were obtained (correlation coefficient, 0.397; R -factor, 0.488; resolution, 15–4.0 Å) by using the program AMoRe (Navaza 1994). We identified two ValRS molecules per asymmetric unit. The structure factor amplitude, phase, and probability of each reflection were calculated by using the programs

sfall and sigmaa (CCP4 1994). The application of density modification procedures, including solvent flattening (55% of the estimated solvent content), histogram matching, and noncrystallographic symmetry averaging, with the program dm (CCP4 1994), improved the quality of the phases enough to yield an electron density map (free R -factor, 0.367; averaged figure of merit, 0.848), where the secondary structures were interpretable. The ligand-free ValRS structure was refined by rigid-body and conjugate gradient minimization refinement procedures with the program CNS (Brunger et al. 1998). All measured data within a resolution of 10.0 and 4.0 Å (with the exception of the random 5% of reflections used for the calculation of R_{free}) were used in the refinement. The C α coordinates of the preliminary ligand-free ValRS structure have been deposited in the Protein Data Bank, with the PDB code 1IYW.

Kinetic analysis of tRNA^{Val} mutants

The DNA templates of the *T. thermophilus* tRNA^{Val} mutants were amplified using a PCR technique, and were cloned into the pUC119 plasmid (Takara). Each tRNA mutant was transcribed in vitro, as described by Fukai et al. (2000), and was purified by 10% polyacrylamide gel electrophoresis with 6 M urea. The tRNA mutants were extracted from the gel using a BioTrapTM membrane (Schleicher and Schuell). The valylation reactions were performed at 65°C. The final concentrations of the components of each valylation reaction mixture were 50 mM Tris (pH 7.7), 2.5 mM magnesium chloride, 10 mM potassium chloride, 2.0 mM adenosine triphosphate (ATP), 200 μM L-[U-14C]valine (9.7 GBq/mmol, Moravsek), the *T. thermophilus* tRNA^{Val}(CAC) mutants (0.25–8.0 μM for the wild type and the G18U mutant, 0.5–8.0 μM for the G19C/C56G mutant, and 4–64 μM for the G19C and G18U/G19C mutants), and ValRS (3 nM for the wild type and the G18U mutant, and 8.8 nM for the G19C mutant).

Each reaction was initiated by the addition of ATP, and was terminated by transferring the reaction mixture to one-half of a Whatman 3MM paper filter (ϕ 2.4 cm), which had previously been soaked with 100 μL of 5% trichloroacetic acid (TCA) and dried. The filter was washed three times with ice-cold 5% TCA and twice with ethanol, then dried, and its radioactivity was counted in a liquid scintillation counter. Trials were performed at least twice for each mutant, except for the G18U/G19C mutant. Kinetic parameters were estimated using a Michaelis-Menten plot. Curve-fitting was performed by DeltaGraph (SPSS Science) or Origin 7.0 (Origin).

Kinetic analysis of ValRS mutants

The genes of the *T. thermophilus* ValRS deletion mutants $\Delta(712-862)$ and $\Delta(795-862)$ were amplified by PCR and cloned into the originally constructed T7 expression vector, pK-7 (Kigawa et al. 1995). The R818A/R843A mutation was introduced into the *T. thermophilus* ValRS gene by PCR. *E. coli* strain JM109(DE3) was transformed with each of the expression vectors, and the ValRS mutants were overproduced. The overproduced $\Delta(712-862)$, $\Delta(795-862)$, and R818A/R843A mutants were stably purified by heat-treatment at 70°C for 30–60 min and subsequently by two-step column chromatography, as well as was wild-type *T. thermophilus* ValRS (Fukai et al. 2000). After purification, glycerol was

added to all sample solutions to a final concentration of 50%, and the samples were stored at -20°C . Before the aminoacylation assay, the glycerol in the sample solutions was diluted by dialysis against 25 mM Tris-Cl buffer (pH 7.8), containing 5 mM magnesium acetate, and 5 mM β -mercaptoethanol. The *T. thermophilus* tRNA^{Val}(CAC) transcript was prepared as described above. The native tRNA^{Val} from *T. thermophilus* was a gracious gift from Dr. M. Tukaro (EMBL, Grenoble).

The aminoacylation reactions were performed as described above. The concentration of the *T. thermophilus* tRNA^{Val}(CAC) transcript was adjusted to 0.25–4.0 μM for the wild-type ValRS and 4.0–64 μM for the R818A/R843A and Δ (795–862) mutants, and that of ValRS was adjusted to 5.0 nM for the wild-type ValRS and the R818A/R843A mutant, and 500 nM for the Δ (795–862) mutant. The concentration of the native tRNA^{Val} was adjusted to 0.25–8.0 μM for the wild-type ValRS, 2.0–40 μM for the R818A/R843A mutant, and 4.0–40 μM for the Δ (795–862) mutant, and that of ValRS was adjusted to 5.0–9.0 nM for the wild-type ValRS, 5.0–18 nM for the R818A/R843A mutant, and 0.50–1.8 μM for the Δ (795–862) mutant.

Figure preparation

The molecular graphics in Figures 1–4 were prepared with the programs MOLMOL (Koradi et al. 1996), MOLSCRIPT (Kraulis 1991), O (Jones et al. 1991), Que (<http://www.biochem.s.u-tokyo.ac.jp/~ishitani/que/index-en.html>), Grasp (Nicholls et al. 1991), and Raster3D (Merritt and Bacon 1997).

ACKNOWLEDGMENTS

We thank Dr. Mikhail Tukalo for kindly providing the mature tRNA^{Val} purified from *T. thermophilus*, Drs. Hitoshi Kurumizaka and Mikako Shirouzu and Mr. Kouichiro Kodama for assistance with the experiment using the radioisotope at RIKEN, Dr. Makoto Kitabatake for helpful advice on the steady-state kinetics of the aminoacylation, and Dr. Atsushi Nakagawa for help in data collection at BL44XU in SPring8 (Harima, Japan). This work was supported in part by Grants-in-Aid for Scientific Research on Priority Areas (09278101 and 11169204) to S.Y. and O.N., respectively, from the Ministry of Education, Science, Culture and Sports of Japan. S.F. was supported by Research Fellowships of the Japan Society for the Promotion of Science for Young Scientists.

The publication costs of this article were defrayed in part by payment of page charges. This article must therefore be hereby marked “advertisement” in accordance with 18 USC section 1734 solely to indicate this fact.

Received June 4, 2002; accepted September 23, 2002.

REFERENCES

- Brunger, A.T., Adams, P.D., Clore, G.M., DeLano, W.L., Gros, P., Grosse-Kunstleve, R.W., Jiang, J.S., Kuszewski, J., Nilges, M., Pannu, N.S., et al. 1998. Crystallography & NMR system: A new software suite for macromolecular structure determination. *Acta Crystallogr.* **54**: 905–921.
- Cavarelli, J., Delagoutte, B., Eriani, G., Gangloff, J., and Moras, D. 1998. L-arginine recognition by yeast arginyl-tRNA synthetase. *EMBO J.* **17**: 5438–5448.
- Collaborative Computational Project No. 4. 1994. The CCP4 suite: Programs for protein crystallography. *Acta Crystallogr.* **D50**: 760–763.
- Chen, J.F., Guo, N.N., Li, T., Wang, E.D., and Wang, Y.L. 2000. CP1 domain in *Escherichia coli* leucyl-tRNA synthetase is crucial for its editing function. *Biochemistry* **39**: 6726–6731.
- Chu, W.C. and Horowitz, J. 1991. Recognition of *Escherichia coli* valine transfer RNA by its cognate synthetase: A fluorine-19 NMR study. *Biochemistry* **30**: 1655–1663.
- Chu, W.C., Feiz, V., Derrick, W.B., and Horowitz, J. 1992. Fluorine-19 nuclear magnetic resonance as a probe of the solution structure of mutants of 5-fluorouracil-substituted *Escherichia coli* valine tRNA. *J. Mol. Biol.* **227**: 1164–1172.
- Cusack, S. 1995. Eleven down and nine to go. *Nat. Struct. Biol.* **2**: 824–831.
- Cusack, S., Yaremchuk, A., and Tukalo, M. 2000. The 2 Å crystal structure of leucyl-tRNA synthetase and its complex with a leucyl-adenylate analogue. *EMBO J.* **19**: 2351–2361.
- Delagoutte, B., Moras, D., and Cavarelli, J. 2000. tRNA aminoacylation by arginyl-tRNA synthetase: Induced conformations during substrates binding. *EMBO J.* **19**: 5599–5610.
- Delarue, M. and Moras, D. 1993. The aminoacyl-tRNA synthetase family: Modules at work. *Bioessays* **15**: 675–687.
- Derrick, W. B. and Horowitz, J. 1993. Probing structural differences between native and *in vitro* transcribed *Escherichia coli* valine transfer RNA: Evidence for stable base modification-dependent conformers. *Nucleic Acids Res.* **BO21**: 948–53.
- Eriani, G., Delarue, M., Poch, O., Gangloff, J., Moras, D. 1990. Partition of tRNA synthetases into two classes based on mutually exclusive sets of sequence motifs. *Nature* **347**: 203–206.
- Fersht, A.R. and Kaethner, M.M. 1976. Mechanism of aminoacylation of tRNA. Proof of the aminoacyl adenylate pathway for the isoleucyl- and tyrosyl-tRNA synthetases from *Escherichia coli* K12. *Biochemistry* **15**: 818–823.
- Fukai, S., Nureki, O., Sekine, S., Shimada, A., Tao, J., Vassilyev, D.G., and Yokoyama, S. 2000. Structural basis for double-sieve discrimination of L-valine from L-isoleucine and L-threonine by the complex of tRNA^{Val} and valyl-tRNA synthetase. *Cell* **103**: 793–803.
- Giegé, R., Sissler, M., and Florentz, C. 1998. Universal rules and idiosyncratic features in tRNA identity. *Nucleic Acids Res.* **26**: 5017–5035.
- Horowitz, J., Chu, W.C., Derrick, W.B., Liu, J.C., Liu, M., and Yue, D. 1999. Synthetase recognition determinants of *E. coli* valine transfer RNA. *Biochemistry* **38**: 7737–7746.
- Jones, T.A., Zou, J.Y., Cowan, S.W., and Kjeldgaard, M. 1991. Improved methods for binding protein models in electron density maps and the location of errors in these models. *Acta Crystallogr.* **A47**: 110–119.
- Kiga, D., Sakamoto, K., Sato, S., Hirao, I., and Yokoyama, S. 2001. Shifted positioning of the anticodon nucleotide residues of amber suppressor tRNA species by *Escherichia coli* arginyl-tRNA synthetase. *Eur. J. Biochem.* **268**: 6207–6213.
- Kigawa, T., Muto, Y., and Yokoyama, S. 1995. Cell-free synthesis and amino acid-selective stable isotope labeling of proteins for NMR analysis. *J. Biomol. NMR* **6**: 129–134.
- Koradi, R., Billeter, M., and Wüthrich, K. 1996. MOLMOL: A program for display and analysis of macromolecular structures. *J. Mol. Graph.* **14**: 51–55.
- Kraulis, P.J. 1991. MOLSCRIPT: A program to produce both detailed and schematic plots of protein structures. *J. Appl. Crystallogr.* **24**: 946–950.
- Lin, L., Hale, S.P., and Schimmel, P. 1996. Aminoacylation error correction. *Nature* **384**: 33–34.
- McClain, W.H. and Foss, K. 1988. Changing the acceptor identity of a transfer RNA by altering nucleotides in a “variable pocket”. *Science* **241**: 1804–1807.
- Mechulam, Y., Schmitt, E., Maveyraud, L., Zelwer, C., Nureki, O., Yokoyama, S., Konno, M., and Blanquet, S. 1999. Crystal structure of *Escherichia coli* methionyl-tRNA synthetase highlights species-

- specific features. *J. Mol. Biol.* **294**: 1287–1297.
- Merritt, E.A. and Bacon, D.J. 1997. Raster3D: Photorealistic molecular graphics. *Methods Enzymol.* **277**: 505–524.
- Muramatsu, T., Nishikawa, K., Nemoto, F., Kuchino, Y., Nishimura, S., Miyazawa, T., and Yokoyama, S. 1988. Codon and amino-acid specificities of a transfer RNA are both converted by a single post-transcriptional modification. *Nature* **336**: 179–181.
- Mursinna, R.S., Lincecum, Jr., T.L., and Martinis, S.A. 2001. A conserved threonine within *Escherichia coli* leucyl-tRNA synthetase prevents hydrolytic editing of leucyl-tRNA^{Leu}. *Biochemistry* **40**: 5376–5381.
- Navaza, J. 1994. AMoRe: An automated package for molecular replacement. *Acta Crystallogr.* **A50**: 157–163.
- Newberry, K. J., Hou, Y. -M., and Perona, J. 2002. Structural origins of amino acid selection without editing by cysteinyl-tRNA synthetase. *EMBO J.* **21**: 2778–2787.
- Nicholls, A., Sharp, K.A., and Honig, B. 1991. Protein folding and association: Insights from the interfacial and thermodynamic properties of hydrocarbons. *Proteins* **11**: 281–296.
- Nureki, O., Niimi, T., Muramatsu, T., Kanno, H., Kohno, T., Florentz, C., Giegè, R., and Yokoyama, S. 1994. Molecular recognition of the identity-determinant set of isoleucine transfer RNA from *Escherichia coli*. *J. Mol. Biol.* **236**: 710–724.
- Nureki, O., Vassilyev, D.G., Tateno, M., Shimada, A., Nakama, T., Fukai, S., Konno, M., Hendrickson, T.L., Schimmel, P., and Yokoyama, S. 1998. Enzyme structure with two catalytic sites for double-sieve selection of substrate. *Science* **280**: 578–582.
- Otwinowski, Z. and Minor, W. 1997. Processing of X-ray diffraction data collected in oscillation mode. *Methods Enzymol.* **276**: 307–326.
- Pallanck, L. and Schulman, L.H. 1991. Anticodon-dependent aminoacylation of a noncognate tRNA with isoleucine, valine, and phenylalanine *in vivo*. *Proc. Natl. Acad. Sci.* **88**: 3872–3876.
- Parthasarathy, R., Ohrt, J.M., and Chheda, G.B. 1977. Modified nucleosides and conformation of anticodon loops: Crystal structure of t⁶A and g⁶A. *Biochemistry* **16**: 4999–5008.
- Rould, M.A., Perona, J.J., and Steitz, T.A. 1991. Structural basis of anticodon loop recognition by glutamyl-tRNA synthetase. *Nature* **352**: 213–218.
- Schulman, L.H. and Pelka, H. 1977. Structural requirements for aminoacylation of *Escherichia coli* formylmethionine transfer RNA. *Biochemistry* **16**: 4256–4265.
- Sekine, S., Nureki, O., Shimada, A., Vassilyev, D.G., and Yokoyama, S. 2001. Structural basis for anticodon recognition by discriminating glutamyl-tRNA synthetase. *Nat. Struct. Biol.* **8**: 203–206.
- Shimada, A., Nureki, O., Goto, M., Takahashi, S., and Yokoyama, S. 2001. Structural and mutational studies of the recognition of the arginine tRNA-specific major identity element, A20, by arginyl-tRNA synthetase. *Proc. Natl. Acad. Sci.* **6**: 6.
- Silvian, L.F., Wang, J., and Steitz, T.A. 1999. Insights into editing from an Ile-tRNA synthetase structure with tRNA^{Ile} and mupirocin. *Science* **285**: 1074–1077.
- Sprinzel, M., Horn, C., Brown, M., Ioudovitch, A., and Steinberg, S. 1998. Compilation of tRNA sequences and sequences of tRNA genes. *Nucleic Acids Res.* **26**: 148–153.
- Sugiura, I., Nureki, O., Ugaji-Yoshikawa, Y., Kuwabara, S., Shimada, A., Tateno, M., Lorber, B., Giegè, R., Moras, D., Yokoyama, S., et al. 2000. The 2.0 Å crystal structure of *Thermus thermophilus* methionyl-tRNA synthetase reveals two RNA-binding modules. *Structure Fold. Des.* **8**: 197–208.
- Sussman, J.L. and Kim, S. 1976. Three-dimensional structure of a transfer RNA in two crystal forms. *Science* **192**: 853–858.
- Tamura, K., Himeno, H., Asahara, H., Hasegawa, T., and Shimizu, M. 1991. Identity determinants of *E. coli* tRNA(Val). *Biochem. Biophys. Res. Comm.* **177**: 619–623.
- Vlassov, V.V., Kern, D., Romby, P., Giegè, R., and Ebel, J.P. 1983. Interaction of tRNA^{Phe} and tRNA^{Val} with aminoacyl-tRNA synthetases. A chemical modification study. *Eur. J. Biochem.* **132**: 537–544.



RNA

A PUBLICATION OF THE RNA SOCIETY

Mechanism of molecular interactions for tRNA^{Val} recognition by valyl-tRNA synthetase

SHUYA FUKAI, OSAMU NUREKI, SHUN-ICHI SEKINE, et al.

RNA 2003 9: 100-111

References

This article cites 43 articles, 7 of which can be accessed free at:
<http://rnajournal.cshlp.org/content/9/1/100.full.html#ref-list-1>

License

Email Alerting Service

Receive free email alerts when new articles cite this article - sign up in the box at the top right corner of the article or [click here](#).

To subscribe to *RNA* go to:
<http://rnajournal.cshlp.org/subscriptions>
